ACS ORGANIC & INORGANIC Au
AN OPEN ACCESS JOURNAL OF THE AMERICAN CHEMICAL SOCIETY

pubs.acs.org/orginorgau

Article

Effects of Ancillary Ligands on Deep Red to Near-Infrared Cyclometalated Iridium Complexes

Po−Ni Lai, Sungwon Yoon, Yumeng Wu, and Thomas S. Teets*

Cite This: *ACS Org. Inorg. Au* 2022, 2, 236−244

Read Online

ACCESS | Metrics & More | Article Recommendations | Supporting Information

ABSTRACT: The design of organometallic compounds with efficient phosphorescence in the deep red to near-infrared portions of the spectrum is a long-standing fundamental challenge. Here we describe a series of heteroleptic bis-cyclometalated iridium complexes with phosphorescence in these low-energy regions of the spectrum. The cyclometalating ligands in this study feature a metalated benzothiophene aryl group substituted with a quinoline, isoquinoline, or phenanthridine heterocycle. Increasing the conjugation on the heterocycle stabilizes the ligand-centered LUMO, decreases the HOMO−LUMO gap, and enables phosphorescence to occur at long wavelengths. These cyclometalating ligands are paired with a variety of electron-rich ancillary ligands, such as dithiocarbamate (dipdtc), β-ketoiminate (acNac), β-diketiminate (NacNac), amidinate (dipba), and hexahydropyrimidopyrimidine (hpp), some of which have significant influences on the phosphorescence wavelength and excited-state dynamics. The syntheses of seven compounds in this series are described, three of which are structurally validated by single-crystal X-ray diffraction. Cyclic voltammetry reveals the effects of ligand modification on the frontier orbital energies. The photophysical properties of all compounds are thoroughly characterized by UV−vis absorption spectroscopy and steady-state photoluminescence at room-temperature and 77 K. Photoluminescence quantum yields and lifetimes of all compounds are reported.

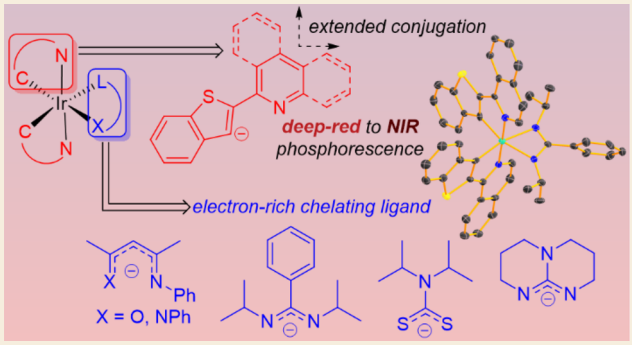

KEYWORDS: *cyclometalated iridium, excited-state dynamics, ligand design, red phosphorescence, deep red phosphorescence, photoluminescence*

INTRODUCTION

Coordination compounds and organometallic compounds with long-lived triplet excited states, most of which luminesce via phosphorescence, have found applications in many subfields of chemistry, biology, and physics, for example, in photoredox catalysis,[1,2] photovoltaics,[3,4] solar fuels,[5,6] and sensing.[7,8] Arguably the most prolific application of phosphorescent metal complexes, and certainly the most lucrative, is organic light-emitting diodes (OLEDs) and other optoelectronic applications.[9] Phosphorescent metal complexes can efficiently harvest both singlet and triplet excitons when used as the emissive dopant in these devices, leading to higher theoretical and practical device efficiencies.[10,11] The discovery over 20 years ago that phosphorescent metal complexes can be used as components in efficient OLED devices has spurred the discovery and investigation of many different types of molecular phosphors.

Of the many classes of phosphorescent metal complexes that have been investigated in OLEDs, cyclometalated iridium complexes have emerged at the forefront and have found commercial success. The photoluminescence quantum yield (Φ_{PL}) of the emissive dopant directly factors in to the OLED device efficiency. Cyclometalated iridium complexes in general have very high quantum yields for phosphorescent emission, and the emission wavelength (color) is easily tuned by changing the cyclometalating ligands. In the middle regions of the visible spectrum, i.e., sky blue, green, yellow, and orange, there are many examples of cyclometalated iridium complexes with near-unity quantum yields.[9,12−15] The deep blue region of the spectrum presents its own set of challenges to achieve efficient and stable blue phosphorescence, which is a subject of active research in several groups.[16−18]

In the red region of the spectrum (peak emission λ = 600−650 nm), there are cyclometalated iridium complexes that function well enough to be incorporated into commercial OLED devices. However, the most efficient OLEDs reported in the academic literature all use cyclometalated iridium

Received: November 1, 2021
Revised: December 28, 2021
Accepted: January 4, 2022
Published: January 20, 2022

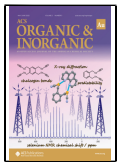

https://doi.org/10.1021/acsorginorgau.1c00044
ACS Org. Inorg. Au 2022, 2, 236−244

dopants with photoluminescence quantum yields ≈0.5,[19−21] falling well short of the near-unity quantum yields achievable in other regions of the spectrum. Thus, it should be possible to realize improvements in red OLED efficiency by discovering red-phosphorescent compounds with higher quantum yields. Moreover, the quantum yields tend to be even lower in compounds that luminesce in the deep red (peak emission λ = 650−700 nm) or near-infrared (NIR, peak emission λ > 700 nm) regions;[22] in the latter case, Φ_{PL} > 0.2 is rare.[23] Although deep red to NIR phosphorescence is not needed for color display applications, there is a long-standing fundamental challenge with achieving high quantum yields in these regions, and there are other applications, including night vision technologies, data security, and bioimaging, that would benefit from the availability of robust and bright deep red to NIR phosphors.

Our group has discovered and elaborated a strategy for efficient photoluminescence in the low-energy regions of the spectrum, preparing heteroleptic bis-cyclometalated iridium complexes supported by nitrogen-containing electron-rich ancillary ligands.[24] Using this strategy, we have prepared red-phosphorescent compounds with record-breaking quantum yields (Φ_{PL} ≈0.8)[25] supported by β-ketoiminate or amidinate ancillary ligands, unveiled key structure−property relationships in a larger suite of related compounds,[26] and made targeted modifications to the ancillary ligands to optimize the deep red phosphorescence.[27] In this work we apply this same strategy to prepare deep red to NIR-phosphorescent complexes where the cyclometalating ligand is a quinoline-, isoquinoline-, or phenanthridine-substituted benzothiophene. As shown in Figure 1, the cyclometalating ligand 2-pyridylbenzothiophene

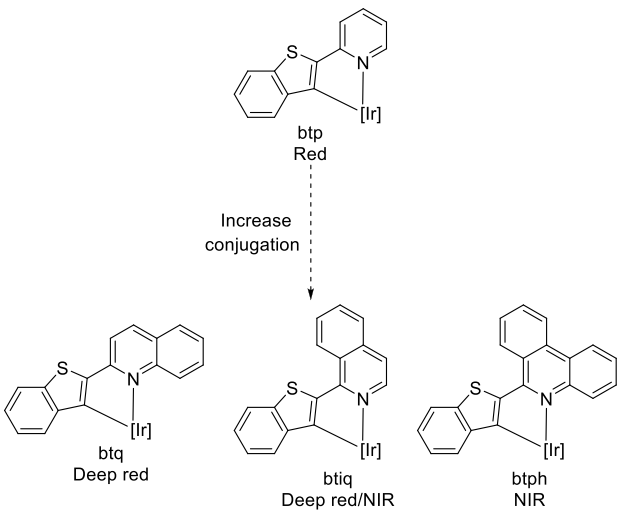

Figure 1. Structures of the cyclometalating ligand btp and the more conjugated analouges btq, btiq, and btph.

(btp) is commonly used to support red-phosphorescent compounds,[21,25,26] and its conjugation can be extended in either or both of two directions on the *N*-heterocycle, resulting in the quinoline (btq),[28] isoquinoline (btiq),[29] and phenanthridine (btph)[23] analogues. We have recently disclosed a set of btph-supported NIR-phosphorescent compounds with a complementary family of quinoline-derived ancillary ligands,[30] and in this work we report compounds where the btq, btiq, and btph cyclometalating ligands in Figure 1 are paired with the electron-rich β-ketoiminate, β-diketiminate, and amidinate ancillary ligands our group has popularized in previous red and deep red designs. In addition to these three ancillary ligand classes, one of the compounds in this work includes a dithiocarbamate ancillary ligand, which was recently used to support red-phosphorescent compounds,[31] and we also introduce hexahydropyrimidopyrimidine (hpp) as an ancillary ligand for bis-cyclometalated iridium. A series of seven new compounds is described, and their photophysical properties are characterized and described in detail. This work shows that the emission wavelengths and excited-state dynamics in these compounds are dependent on the ancillary ligand, and in some cases efficient NIR phosphorescence can be achieved.

RESULTS AND DISCUSSION

Synthesis

A total of seven new compounds partnering the cyclometalating ligands btq, btiq, and btph with different electron-rich ancillary ligands are described in this paper. The general synthetic strategy is shown in Scheme 1, following the methodology we previously employed to synthesize a variety of cyclometalated iridium complexes with electron-rich ancillary ligands.[25−27,32,33] Briefly, the chloro-bridged dimer $[Ir(C^N)_2(\mu\text{-}Cl)]_2$, where C^N is the cyclometalating ligand, is treated with the lithium or potassium salt of the ancillary ligand (L^X) in THF, furnishing the $Ir(C^N)_2(L^X)$ complexes. The electron-rich ancillary ligands β-ketomiminate (acNac), β-diketiminate (NacNac), and amidinate (dipba) have been previously used by our group and were also included in this study. We also include one compound supported by *N*,*N*′-diisopropyldithiocarbamate (dipdtc), which was recently used to support red-phosphorescent iridium complexes.[31,34] In addition, we prepared one complex with hexahydropyrimidopyrimidine (hpp) as an ancillary ligand, which is extensively used as a bridging ligand for metal−metal bonded complexes[35] and is applied here for the first time as an ancillary ligand for cyclometalated iridium complexes. The complexes are abbreviated with the convention "**C^N-L^X**", where C^N is the cyclometalating ligand abbreviation and L^X is the ancillary ligand abbreviation. For example, **btph-acNac** represents the compound $Ir(btph)_2(acNac)$, partnering the cyclometalating ligand btph with the β-ketoiminate ancillary ligand. Some of the **C^N-L^X** combinations we attempted produced intractable product mixtures from which the pure product could not be extracted, but the identity and purity of all complexes in Scheme 1 were ascertained by a combination of ^{1}H NMR (all complexes), $^{13}C\{^1H\}$ NMR (**btph-acNac** and **btph-NacNac**), and high-resolution mass spectrometry. The NMR spectra are displayed in the Supporting Information (Figures S17−S25).

X-ray Crystallography

The molecular structures of three of the seven new compounds were confirmed by single-crystal X-ray diffraction and are shown in Figure 2. Table S1 in the Supporting Information summarizes refinement data. As is typically the case in bis-cyclometalated iridium complexes, the nitrogen atoms of the C^N heterocycles are trans to one another in the distorted octahedral coordination environment. The crystal structures confirm the approximate C_2 symmetry of the **btiq-dipba** and **btph-dipba** complexes, whereas the **btph-acNac** complex is C_1. In the structures where C^N is btph, one of the fused aryl rings on each phenanthridine hangs over the site where the ancillary ligand binds, forming a cleft in which the ancillary ligand

https://doi.org/10.1021/acsorginorgau.1c00044
ACS Org. Inorg. Au 2022, 2, 236−244

Scheme 1. Synthesis of the Complexes Reported in This Study[a]

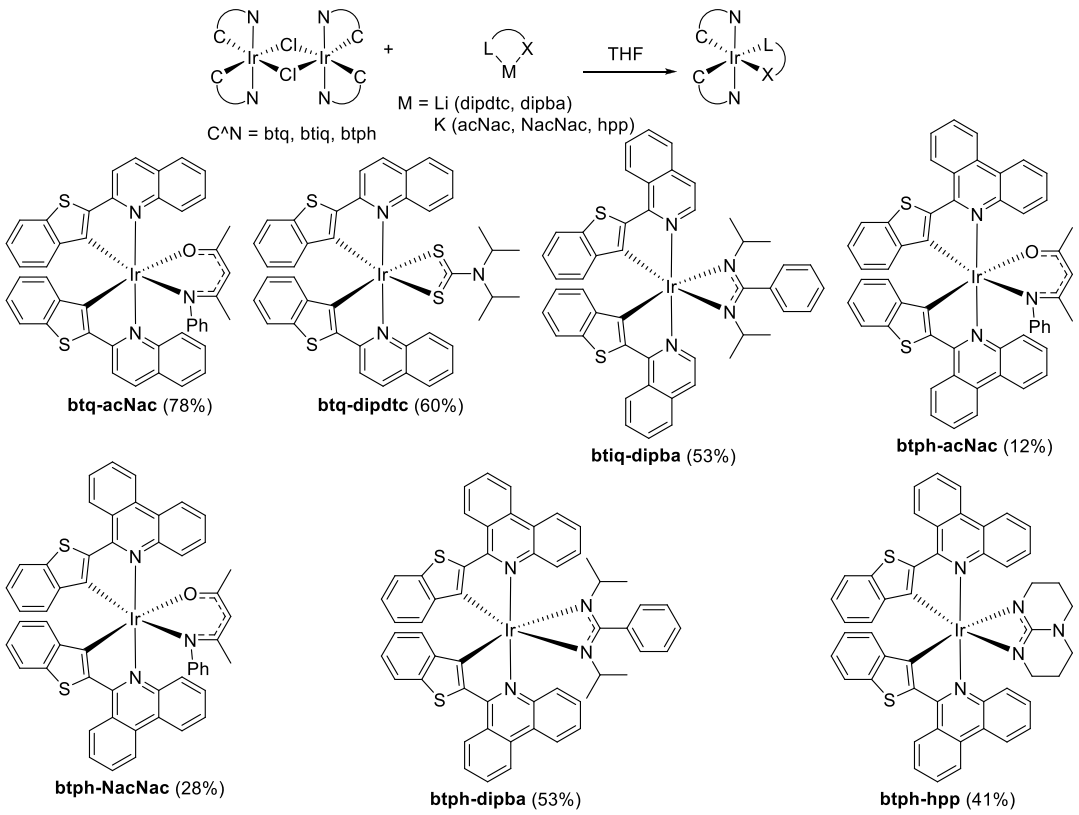

[a]Isolated yields are shown in parentheses.

resides. The btph ligands exhibit a slight twist between the phenanthridine heterocycle and the cyclometalated benzothiophene, likely to alleviate steric pressure. One distinct feature of the **btph-acNac** structure is a puckering of the acNac ancillary ligand, where the backbone carbon atoms of acNac protrude out of the N−Ir−O chelate plane. This degree of puckering was not observed in previously reported Ir(C^N)$_2$(acNac) structures where the C^N ligand was 2-phenylbenzothiazole (pbt), 1-phenylisquinoline (piq), or btp.[25,32] In these previous structures, the C^N ligands did not have a fused aryl ring hanging directly over the ancillary ligand binding pocket, so this puckering may occur to relieve steric interactions between the C^N and L^X ligands. Otherwise, there are no remarkable features of the three crystal structures, with bond lengths and bond angles largely in line with other reported structures from our group that include the same C^N[30] or L^X[25,32] ligands.

Redox Potentials

Our previous work on bis-cyclometalated iridium complexes with electron-rich ancillary ligands established robust trends for the effects of the electron-rich ancillary ligands on the redox potentials and frontier orbital energies.[24] We also recorded cyclic voltammograms of the compounds reported here, with particular interest in how the new ancillary ligands dipdtc and hpp influenced the relevant potentials. Figure S1 of the Supporting Information shows cyclic voltammograms for the seven complexes, and the observed redox potentials are summarized in Figure 3 and Table 1. All values are reported versus the ferrocenium/ferrocene couple (Fc^+/Fc). Scanning anodically, all complexes show a formally Ir^{IV}/Ir^{III} redox wave, which is normally reversible or quasi-reversible. The half-wave potential of this feature is strongly responsive to the identity of the ancillary ligand, shifting more negative as the L^X ligand becomes more electron-rich. The complexes with L^X = dipdtc, acNac, and dipba all have similar Ir^{IV}/Ir^{III} couples, spanning the narrow range from 0.23 (**btiq-dipba**) to 0.36 V (**btph-acNac**). These values are in the range of several other compounds from our group with acNac or dipba ancillary ligands.[25,32] At parity of L^X ligand, the complexes with C^N = btph seem to have the most positive Ir^{IV}/Ir^{III} couples by about 60−70 mV relative to the respective btq or btiq complex. The Ir^{IV}/Ir^{III} potential for **btph-NacNac** is cathodically shifted to +0.07 V, and **btph-hpp** has the most negative value of −0.11 V, suggesting it is the most electron-rich ancillary ligand in the series. To put this latter value in context, we can compare to some related bis-cyclometalated iridium complexes from our group featuring acyclic guanidinate ancillary ligands.[27] The corresponding Ir^{IV}/Ir^{III} potentials for these complexes are +0.01 (C^N = piq) and +0.10 V (C^N = btp), which are more positive by >100 mV than that of **btph-hpp**. To explain this, we refer to other experimental and computational work from our group,[25,36] which shows that increasing the electron richness of the ancillary ligand increases its contribution to the HOMO, raises the energy of the HOMO, and cathodically shifts the Ir^{IV}/Ir^{III} couple. We note that the uncoordinated nitrogen atom in acyclic guanidinates can in principle rotate out of conjugation with the amidinate core, which is prevented in **hpp** due to its fused bicyclic nature. Thus, in **hpp** the stronger conjugation of the uncoordinated nitrogen atom lone pair increases the ligand electron density. Scanning in the negative direction, one or two reversible waves were observed that corresponded to the reduction of the C^N ligands. The

https://doi.org/10.1021/acsorginorgau.1c00044
ACS Org. Inorg. Au 2022, 2, 236−244

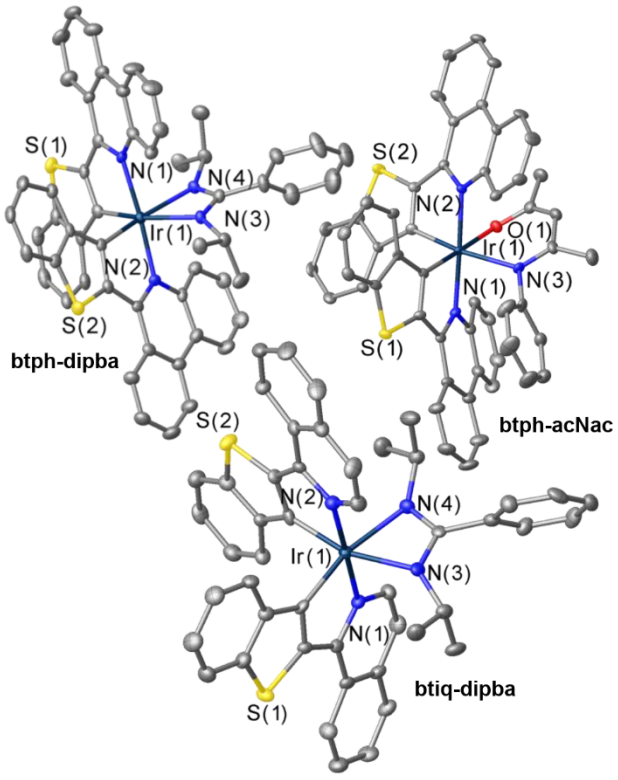

Figure 2. Molecular structures of **btiq-dipba, btph-acNac**, and **btph-dipba** determined by single-crystal X-ray diffraction. The solvent molecules and hydrogen atoms are omitted from the structures, and ellipsoids are shown at the 50% probability level.

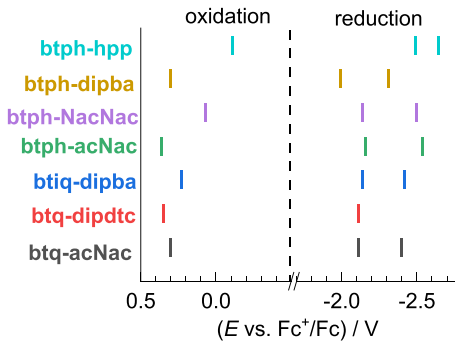

Figure 3. Summary of the redox potentials of the complexes described here, with each vertical line representing the half-wave potential for the observed oxidation and reduction waves.

potentials for these waves in most cases are not very responsive to the L^X ligand and are similar across the series of complexes. An exception is the complex **btph-hpp** in which the reduction waves are less clearly resolved but appear to be shifted to substantially more negative potentials, in particular the first reduction that is ca. 0.3 V more negative than any of the other compounds. Nevertheless, the electrochemical data are consistent with these compounds having frontier orbital compositions typical of bis-cyclometalated iridium complexes, with a delocalized HOMO that consists of significant contributions from the L^X ligand, the cyclometalated aryl ring, and the Ir 5dπ orbitals and a LUMO that is localized on the *N*-heterocycle of the C^N ligand.

Photoluminescence

The UV−vis absorption spectra of all complexes are collected in Figures S2−S8 in the Supporting Information, and they display the features typically seen in the spectra of related compounds.[13,21,37,38] Strong transitions in the UV region are assigned to ligand-localized $\pi \rightarrow \pi^*$ transitions. The near-UV to blue region features slightly weaker transitions that are assigned to intraligand charge-transfer states, and in the visible region there are even weaker $^{1/3}$MLCT transitions tailing out beyond 600 nm. The absorption spectra do not differ dramatically between the seven complexes, and inspecting the spectra of the C^N = btph series (Figure S9) reveals only subtle influences of the L^X ligand.

Excitation of the compounds in their absorption window (see Figures S10−S16 for excitation spectra) produces photoluminescence in the deep red to near-infrared regions. The photoluminescence spectra, recorded in THF at room temperature and in toluene at 77 K, are shown in Figure 4. The two btq complexes luminesce in the deep red region, with peak wavelengths of 661 (L^X = dipdtc) and 673 nm (L^X = acNac) that depend slightly on the ancillary ligand. For these complexes, the photoluminescence quantum yields are modest, 0.052 for **btq-acNac** and 0.012 for **btq-dipdtc**, largely on account of small radiative rate constants (k_r) of these compounds (see Table 1). In the complex **btiq-dipba**, where the isomeric isoquinoline-based C^N ligand was used, the photoluminescence is substantially red-shifted, with a peak wavelength of 720 nm at room temperature. For this compound Φ_{PL} = 0.14, representing a moderate value for this region of the spectrum. Interestingly, in the compounds with C^N = btph, an analogue of btiq with an additional fused ring (see Figure 1), the photoluminescence does not shift further into the red. The four btph compounds have peak PL wavelengths that are either slightly red-shifted (L^X = acNac and NacNac) or slightly blue-shifted (L^X = dipba and hpp)

Table 1. Summary of electrochemical and photoluminescence data

	cyclic voltammetry		photoluminescence					
compound	E_{ox}/V[a]	E_{red}/V[a]	λ (nm) (RT)[b]	λ (nm) (77 K)[c]	Φ_{PL} (RT)	τ/μs (RT)	$k_r \times 10^{-5}$ (s^{-1})	$k_{nr} \times 10^{-5}$ (s^{-1})
btq-acNac	+0.30	−2.11, − 2.40	673, 731(sh)	661, 728, 812	0.052	2.7	0.19	3.5
btq-dipdtc	+0.35	−2.11	661, 719(sh)	647, 710, 787	0.012	1.4	0.086	7.1
btiq-dipba	+0.23	−2.14, − 2.42	720, 785(sh)	702, 772	0.14	1.2	1.2	7.2
btph-acNac	+0.36	−2.16, − 2.54	722, 790(sh)	709, 784	0.28	1.6	1.8	4.5
btph-NacNac	+0.07	−2.14, − 2.50	733	717, 788	0.078	0.69	1.1	13
btph-dipba	+0.30	−1.99, − 2.31	713, 786(sh)	703, 777	0.25	2.3	1.1	3.3
btph-hpp	−0.11	−2.49, − 2.64	716, 787(sh)	702, 775	0.14	1.4	1.0	6.1

[a]In MeCN, referenced to the ferrocenium/ferrocene couple. [b]In THF. [c]In toluene.

https://doi.org/10.1021/acsorginorgau.1c00044
ACS Org. Inorg. Au 2022, 2, 236−244

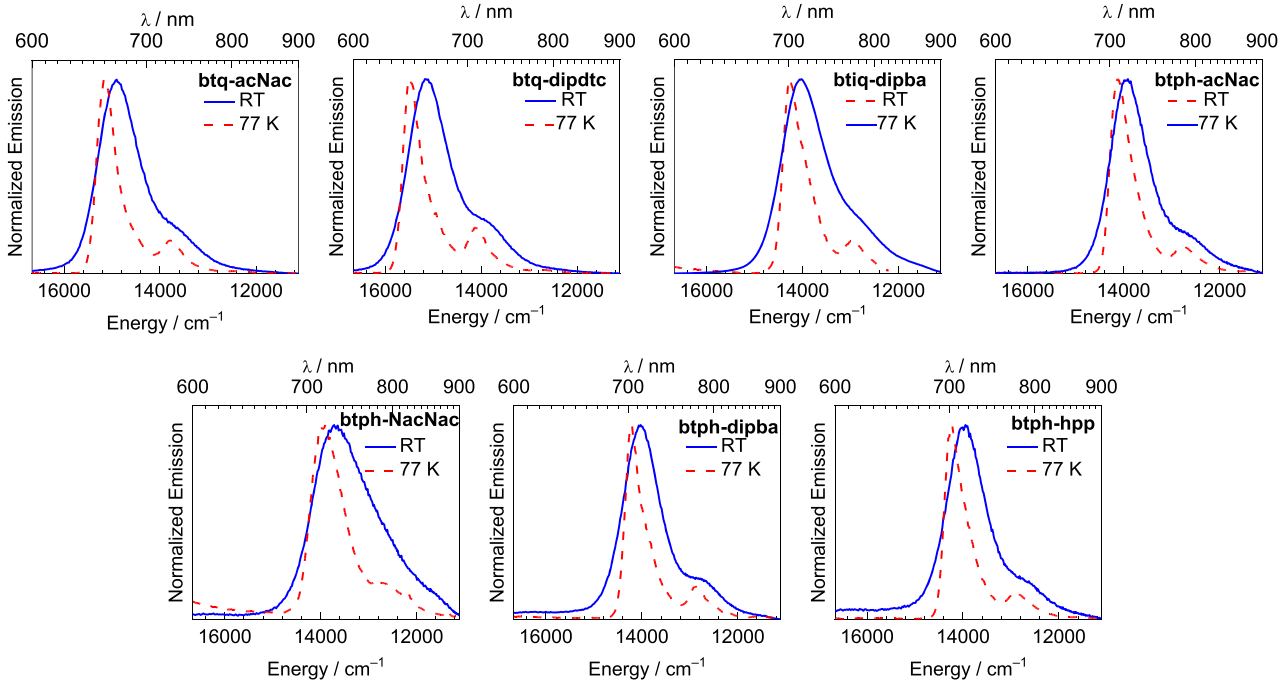

Figure 4. Photoluminescence spectra of all complexes recorded in THF at room temperature (blue solid line) and toluene at 77 K (red dashed line). Samples were excited at 420 nm for all experiments.

relative to **btiq-dipba**, but overall are very similar. This observation indicates that either the second fused ring in btph has very little effect on the LUMO delocalization and energy or the slight twist of the btph ligand (see Figure 2 and the accompanying discussion) obviates any potential increase in the conjugation.

Nevertheless, the four compounds with C^N = btph more clearly reveal the effects of the ancillary ligand on the excited-state dynamics. All four btph complexes have similar k_r values spanning 1.1−1.8 × 10^5 s^{-1}, with the largest k_r value found in **btph-acNac** allowing it to have the highest quantum yield in the series (0.28). The nonradiative rate constant (k_{nr}) is quite responsive to the L^X ligand, with **btph-NacNac** having the largest k_{nr} value (1.3 × 10^6 s^{-1}) and thus the smallest Φ_{PL} (0.078) of the btph series. We previously observed large k_{nr} values in NacNac-supported complexes,[25] which can in principle be mitigated to some extent with a more sterically crowded NacNac analogue.[27] In all complexes in this series, the PL spectra recorded at 77 K exhibit a modest rigidochromic blue-shift of 200−350 cm^{-1} and a more pronounced vibronic structure, which is consistent with a T_1 state that has mixed ligand-centered (^{3}LC) and metal-to-ligand charge transfer (^{3}MLCT) character.[39]

Comparing the photoluminescence data from the compounds in this study with those of several other compounds from our group and others reveals that the electron-rich ancillary ligands we used here are not particularly beneficial to the photoluminescence in these compounds. The complexes **btq-acNac** and **btq-dipdtc** both have significantly lower Φ_{PL} values than the respective homoleptic *fac*-Ir(btq)$_3$[28] and heteroleptic Ir(btq)$_2$(acac)[40] complexes. The spectrum of **btiq-dipba** is red-shifted by 10 nm (200 cm^{-1}) relative to that of Ir(btiq)$_2$(acac),[40] with an identical quantum yield (Φ_{PL} = 0.14) and a slightly shorter lifetime (1.2 versu 1.4 μs). The photoluminescence quantum yields of **btph-acNac** and **btph-dipba** rival those of other top-performing NIR phosphors with the same cyclometalating ligand,[23,30] but again there is no obvious benefit from the electron-rich ancillary ligands. Table 2 compares key photoluminescence data for **btph-acNac** and **btph-dipba**, the two compounds with the highest quantum yields in this work, to closely related red-emitting examples from our group that use the same ancillary ligands. We have previously shown that, with rare exceptions, the excited-state dynamics of red-emitting btp complexes (Figure 1) are not beneficially influenced by electron-rich ancillary ligands,[25,27] and this work shows that the same trend holds true for the π-extended btq, btiq, and btph analogues. Our larger body of work shows that when C^N ligands with cyclometalated phenyl rings are used, the radiative rate constant k_r is augmented when electron-rich L^X ligands are used, and increases in Φ_{PL} often occur.[25−27] However, with benzothiophene-derived C^N ligands like those used here,[25−27,30] k_r is lagely unresponsive to the nature of the ancillary ligand, so control over k_{nr} becomes critical for optimizing Φ_{PL}.

Table 2. Summary of Select Room-Temperature Photoluminescence Data for btph-acNac and btph-dipba Compared to Red-Emitting Analogues Previously Published by Our Group

complex	λ (nm)	Φ_{PL}	τ (μs)	$k_r \times 10^{-5}$ (s^{-1})
piq-acNac[25]	637	0.80	1.0	8.0
piq-dipba[25]	671	0.34	0.71	4.6
btp-acNac[25]	614	0.33	5.8	0.57
btp-dipba[25]	622	0.79	5.3	1.5
btph-acNac	722, 790(sh)	0.28	1.6	1.8
btph-dipba	713, 786(sh)	0.25	2.3	1.1

CONCLUSIONS

This work presents seven new deep red to near-infrared bis-cyclometalated iridium complexes with electron-rich ancillary

https://doi.org/10.1021/acsorginorgau.1c00044
ACS Org. Inorg. Au 2022, 2, 236−244

ligands. The complexes were prepared by a general route and feature varying combinations of three cyclometalating ligands and five ancillary ligands. Electrochemical studies indicate that the HOMO energy is profoundly and systematically influenced by the ancillary ligand, whereas the C^N-localized LUMO is affected to a lesser extent and not in a predictable fashion. All complexes are luminescent at room temperature and in the deep red (C^N = btq) or NIR (C^N = btiq or btph) regions when cooled to 77 K. The btq complexes have modest photoluminescence quantum yields, whereas the btiq and btph compounds have moderate to good quantum yields. Four different ancillary ligands were used for the btph series, and across this subset the k_r values were generally quite similar, so the observed Φ_{PL} was strongly dependent on the magnitude of k_{nr}. Some of the compounds in this study have quantum yields that rival previous state-of-the-art examples, but there is no readily apparent benefit of pairing electron-rich ancillary ligands with the benzothiophene-derived C^N ligand class used in this work. Continued development of top-performing NIR cyclometalated iridium phosphors will require either better strategies for controlling and minimizing k_{nr} or alternative C^N ligands that enable the radiative rates to be more strongly influenced by the ancillary ligand.

EXPERIMENTAL SECTION

Materials

The cyclometalating ligand precursors for btq, btiq, and btph were prepared via Suzuki coupling reactions as previously described.[23] The chloride-bridged cyclometalated iridium dimers $[Ir(C^N)_2(\mu\text{-}Cl)]_2$ were prepared by the method of Nonoyama,[41] refluxing $IrCl_3{\cdot}xH_2O$ with 2−2.5 equiv of the cyclometalating ligand in a mixed 2-ethoxyethanol/water solvent system. The alkali metal salts of the acNac, NacNac, and dipba ancillary ligands were prepared as previously described by our group.[25,32] Similarly, the potassium salt of hpp (hppK) was prepared by the deprotonation of hexahydropyrimidopyrimidine with benzyl potassium. The lithium salt of dipdtc (Lidipdtc) was prepared by a literature procedure.[42] Solvents for reactions, electrochemical measurements, and photophysical experiments were dried using a Grubbs solvent purification system with dual aluminum columns and stored over 3 Å molecular sieves in a glovebox. Deuterated NMR solvents were obtained from Cambridge Isotope Laboratories and stored over 3 Å molecular sieves. Tetrabutylammonium hexafluorophosphate was recrystallized from methanol and ferrocene-sublimed before use in electrochemical experiments.

Physical Methods

For all compounds, two or more physical methods were used to verify their identity and purity. ^{1}H NMR spectra of all compounds are consistent with their structures and suggestive of bulk purity. The complexes **btph-acNac** and **btph-NacNac** were sufficiently soluble for $^{13}C\{^1H\}$ NMR analysis, whereas for the rest high-resolution ESI mass spectrometry was used as an additional tool to ascertain the compound identity. NMR spectra were recorded on a JEOL ECA-500 or ECA-600 spectrometer at room temperature. Cyclic voltammograms were recorded with a CHI 602E potentiostat interfaced to a nitrogen glovebox via wire feedthroughs. Samples were dissolved in MeCN with 0.1 M tetrabutyl hexafluorophosphate as the electrolyte. A 3 mm diameter glassy carbon working electrode, a platinum wire counter electrode, and a silver wire pseudoreference electrode were used. Potentials were referenced to an internal standard of ferrocene. Prior to collecting the CV of each complex, a blank scan on just the solvent and the electrolyte was conducted to ensure there was no appreciable background current. In a typical experiment, a clean baseline was observed in the potential range from +0.9 to −3.1 V versus Fc^+/Fc, with all of the observed CV features (Figure 3) falling well within this range. Samples for UV−vis absorption and room-temperature photoluminescence measurements were prepared in a nitrogen-filled glovebox and contained in quartz cuvettes with threaded screw-cap enclosures. Samples for photoluminescence measurements at 77 K were prepared in a custom quartz EPR tube with a high-vacuum Teflon valve and immersed in liquid nitrogen using a finger dewar. UV−vis absorption spectra were recorded using an Agilent Carey 8454 UV−vis spectrophotometer, and steady-state photoluminescence spectra were recorded using a Horiba FluoroMax-4 spectrofluorometer. Photoluminescence quantum yields were determined relative to a standard of tetraphenylporphyrin (TPP) in toluene, which has a fluorescence quantum yield of 0.11.[43] Photoluminescence lifetimes were recorded on a Horiba DeltaFlex Lifetime System using 430 nm pulsed diode excitation.

X-ray Crystallography Details

Single crystals were grown by vapor diffusion. Crystals were mounted on a Bruker Apex II three-circle diffractometer using Mo Kα radiation (λ = 0.71073 Å). The data were collected at 123(2) K and processed and refined within the APEXII software. Structures were solved by intrinsic phasing in SHELXT and refined by standard difference Fourier techniques in the program SHELXL.[44] Hydrogen atoms were placed in calculated positions using the standard riding model and refined isotropically; all non-hydrogen atoms were refined anisotropically. The structure of **btiq-dipba** included two disordered CH_2Cl_2 solvent molecules, each modeled as two-part disorders. The structure of **btph-acNac** included heavily disordered solvent electron density that could not be satisfactorily refined, necessitating the use of the SQUEEZE function in PLATON.[45] The structure of **btph-dipba** included a disordered pentane molecule, which was modeled as a two-part disorder with a 50% total occupancy. The bond distances and angles in all disordered parts were restrained using SADI commands, and the ellipsoid parameters were restrained with the rigid-bond restraints SIMU and DELU. Crystallographic details are summarized in Table S1.

Synthesis of btq-acNac

In the glovebox, $[Ir(btq)_2(\mu\text{-}Cl)]_2$ (31 mg, 0.021 mmol) was suspended in 2 mL of THF. A solution of acNacK (20 mg, 0.094 mmol, 4.3 equiv) in 5 mL of THF was added to the stirred mixture. The resulting dark pink mixture was stirred for 2 h at room temperature, during which time the solids were drawn into solution and a dark purple solution resulted. The solvent was evaporated, and the resulting residue was extracted with 5 mL of toluene and filtered through Celite. The toluene was removed in vacuo, and the residue was triturated with 2 mL of room-temperature Et_2O before the red product was filtered off. The solid was collected from the filter by dissolving it in THF, and the resulting solution was concentrated to dryness. Finally, the crude product was washed and dissolved in a minimum amount of THF, and pentane was slowly added to precipitate out the purple solids. The solids were filtered and dried. Yield: 28 mg (78%). ^{1}H NMR (500 MHz, C_6D_6) δ: 9.26 (d, J = 9.0 Hz, 1H, ArH), 8.85−8.91 (m, 1H, ArH), 7.53 (d, J = 8.5 Hz, 1H, ArH), 7.48 (d, J = 8.0 Hz, 1H, ArH), 7.43 (d, J = 8.5 Hz, 1H, ArH), 7.39 (d, J = 8.0 Hz, 1H, ArH), 7.27 (d, J = 9.0 Hz, 2H, ArH), 7.24 (d, J = 8.0 Hz, 1H, ArH), 6.96−7.07 (m, 5H, ArH), 6.89 (t, J = 7.5 Hz, 1H, ArH), 6.81 (dt, J = 7.1, 21 Hz, 2H, ArH), 6.70 (t, J = 7.3 Hz, 1H, ArH), 6.62 (t, J = 7.5 Hz, 1H, ArH), 6.54 (d, J = 8.5 Hz, 1H, ArH), 6.39−6.49 (m, 3H, ArH), 6.33 (t, J = 7.3 Hz, 1H, ArH), 5.33 (d, J = 8.0 Hz, 1H, ArH), 4.26 (s, 1H, $PhNC(CH_3)CHC(O)CH_3$), 1.62 (s, 3H, CH_3), 1.21 (s, 3H, CH_3). HRMS-ESI (m/z): $[M + Na]^+$ calcd for $C_{45}H_{32}IrN_3OS_2$, 910.1508; found, 910.1505.

Synthesis of btq-dipdtc

$[Ir(btq)_2(\mu\text{-}Cl)]_2$ (10 mg, 0.0067 mmol) was reacted with Lidipdtc (11 mg, 0.062 mmol, 10 equiv) for 30 min at room temperature in 2 mL of THF. The mixture became a dark pink solution. Afterward, the solution was concentrated, and 2 mL of toluene was added to the resulting residue, which was passed through Celite. The toluene solution was evaporated to dryness. The remaining residue was flushed through a short silica column using DCM/hexane (1:1) as the eluent (R_f = 0.7). The solution was evaporated to dryness, and 2 mL

https://doi.org/10.1021/acsorginorgau.1c00044
ACS Org. Inorg. Au 2022, 2, 236−244

of diethyl ether was added to form a pinkish red mixture. The solids were filtered and dried under vacuum. Yield: 7.1 mg (60%). ^{1}H NMR (600 MHz, C_6D_6) δ: 9.02 (d, J = 9.0 Hz, 2H, ArH), 7.54 (dd, J = 8.4, 29 Hz, 4H, ArH), 7.35 (d, J = 7.8 Hz, 2H, ArH), 7.22 (s, 1H, ArH), 7.05 (d, J = 7.8 Hz, 2H, ArH), 6.96 (s, 1H, ArH), 6.83 (t, J = 7.5 Hz, 2H, ArH), 6.71−6.77 (m, 4H, ArH), 6.38 (t, J = 7.8 Hz, 2H, ArH), 5.13 (br, s, 4H, $(CH_3)_2CHN$), 0.61 (br, s, 12H, CH_3). HRMS-ESI (m/z): $[M + Na]^+$ calcd for $C_{41}H_{34}IrN_3S_4$, 912.1153; found, 912.1152.

Synthesis of btiq-dipba

In the glovebox, bromobenzene (50 mg, 0.32 mmol) in 2 mL of THF was first cooled in a coldwell filled with liquid nitrogen. To the mixture was added a hexane solution of *n*-BuLi (0.12 mL, 2.5 M), and the reaction mixturewas stirred in the coldwell for 30 min. The reaction mixture was then added dropwise to *N,N′*-diisopropylcarbodiimide (DIC) (39 mg, 0.32 mmol). The colorless solution was stirred inside the coldwell for another 30 min and then added dropwise to a Teflon-capped glass tube containing $[Ir(btiq)_2(\mu\text{-Cl})]_2$ (50 mg, 0.033 mmol) in 2 mL of THF, which was sealed and removed from the glovebox. After stirring at 80 °C overnight, the reaction mixture was cooled to room temperature, and the volatiles were removed. The crude product was redissolved in a minimum amount of THF and slowly added to pentane to precipitate out the dark solid. The product was triturated with diethyl ether and pentane. Yield: 38 mg (53%). ^{1}H NMR (500 MHz, CD_2Cl_2) δ: 9.47 (d, J = 6.5 Hz, 2H, ArH), 8.96−9.02 (m, 2H, ArH), 8.01−8.07 (m, 2H, ArH), 7.74−7.80 (m, 4H, ArH), 7.70 (d, J = 8.0 Hz, 2H, ArH), 7.61 (d, J = 6.5 Hz, 2H, ArH), 7.25−7.45 (m, 5H, ArH), 7.03 (t, J = 7.0 Hz, 2H, ArH), 6.65 (t, J = 7.8 Hz, 2H, ArH), 6.39 (d, J = 8.0 Hz, 2H, ArH), 3.19 (quint, J = 6.3 Hz, 2H, $(CH_3)_2CHN$), 0.52 (d, J = 6.0 Hz, 6H, CH_3), − 0.20 (d, J = 6.5 Hz, 6H, CH_3). HRMS-ESI (m/z): $[M + H]^+$ calcd for $C_{47}H_{39}IrN_4S_2$, 917.2318; found, 917.2319.

Synthesis of btph-acNac

In the glovebox, $[Ir(btph)_2(\mu\text{-Cl})]_2$ (50 mg, 0.029 mmol) was suspended in 2 mL of THF. A solution of acNacK (30 mg, 0.074 mmol, 2.6 equiv) in 5 mL of THF was added to the stirred mixture. The resulting dark red mixture was stirred overnight at room temperature. The solvent was evaporated, and the resulting residue was extracted with 5 mL of toluene and filtered through Celite. The toluene was removed in vacuo, and the residue was triturated with 2 mL of room-temperature Et_2O before the red product was filtered off. The solid was collected from the filter by dissolving it in DCM, and the resulting solution was concentrated to dryness. Finally, the crude product washed dissolved in minimum amount of THF, and pentane was slowly added to precipitate out the solids. The solids were filtered and dried. Yield: 6.7 mg (12%). ^{1}H NMR (500 MHz, C_6D_6) δ: 9.53 (d, J = 8.5 Hz, 1H, ArH), 9.12 (d, J = 9.0 Hz, 1H, ArH), 8.85−8.91 (m, 1H, ArH), 8.54 (d, J = 9.0 Hz, 1H, ArH), 8.27 (dd, J = 7.3, 21.3 Hz, 2H, ArH), 8.05 (dd, J = 7.8, 22.8 Hz, 2H, ArH), 7.46 (d, J = 8.0 Hz, 1H, ArH), 7.24−7.41 (m, 5H, ArH), 7.20 (d, J = 8.5 Hz, 1H, ArH), 7.11 (s, 1H, ArH), 6.89−7.03 (m, 4H, ArH), 6.87 (d, J = 8.0 Hz, 1H, ArH), 6.56−7.65 (m, 2H, ArH), 6.51 (dt, J = 7.3, 24.3 Hz, 2H, ArH), 6.29 (t, J = 7.8 Hz, 1H, ArH), 6.13 (t, J = 7.3 Hz, 1H, ArH), 5.81 (t, J = 7.5 Hz, 1H, ArH), 6.29 (t, J = 7.8 Hz, 1H, ArH), 5.41 (d, J = 7.5 Hz, 1H, ArH), 4.09 (s, 1H, $PhNC(CH_3)CHC(O)CH_3$), 1.43 (s, 3H, CH_3), 1.04 (s, 3H, CH_3). $^{13}C\{^1H\}$ NMR (151 MHz, CD_2Cl_2) δ: 179.4, 168.9, 168.4, 166.2, 164.8, 161.4, 146.8, 146.2, 146.12, 146.11, 146.06, 143.3, 138.9, 138.8, 133.8, 133.7, 132.1, 131.8, 129.1, 129.0, 128.2, 127.9, 127.7, 127.6, 127.0, 126.9, 126.6, 126.4, 125.9, 125.4, 125.2, 125.0, 124.4, 124.3, 123.8, 123.64 123.5, 122.9, 122.5, 122.0, 121.7, 121.6, 120.8, 101.3, 25.8, 25.0.

Synthesis of btph-NacNac

In the glovebox, $[Ir(btph)_2(\mu\text{-Cl})]_2$ (50 mg, 0.029 mmol) was suspended in 2 mL of THF. A solution of NacNacK (59 mg, 0.203 mmol, 7 equiv) in 5 mL of THF was added to the stirred mixture. The resulting red mixture was stirred overnight at room temperature. The solvent was evaporated, and the resulting residue was extracted with 5 mL of toluene and filtered through Celite. The toluene was removed in vacuo, and the residue was triturated with 2 mL of room-temperature Et_2O before the red product was filtered off. The solid was collected from the filter by dissolving it in DCM, and the resulting solution was concentrated to dryness. The crude product was dissolved in minimum amount of THF and slowly added to pentane to precipitate out the solids. Finally, the crude product washed dissolved in minimum amount of DCM, and hexane was slowly added to precipitate out the solids. The solids were filtered and dried. Yield: 17 mg (28%). ^{1}H NMR (500 MHz, C_6D_6) δ: 10.36 (d, J = 8.5 Hz, 2H, ArH), 8.83 (d, J = 8.0 Hz, 2H, ArH), 8.32 (d, J = 8.5 Hz, 2H, ArH), 8.28 (d, J = 8.5 Hz, 2H, ArH), 7.80 (t, J = 7.0 Hz, 2H, ArH), 7.43 (t, J = 7.5 Hz, 2H, ArH), 7.27 (t, J = 7.8 Hz, 2H, ArH), 7.13 (d, J = 8.0 Hz, 2H, ArH), 7.07 (t, J = 7.8 Hz, 2H, ArH), 6.55−6.61 (m, 4H, ArH), 6.23 (t, J = 7.3 Hz, 2H, ArH), 6.02−6.13 (m, 10H, ArH), 5.19 (s, 1H, $PhNC(CH_3)CHC(CH_3)NPh$), 1.64 (s, 6H, CH_3). $^{13}C\{^1H\}$ NMR (151 MHz, CD_2Cl_2) δ: 170.8, 165.2, 157.9, 151.9, 146.7, 144.3, 139.6, 134.0, 132.0, 130.3, 128.9, 128.8, 127.5, 127.1, 126.3, 125.9, 125.3, 124.8, 124.4, 123.1, 122.3, 122.2, 122.1, 121.0, 121.0, 99.3, 24.7.

Synthesis of btph-dipba

In the glovebox, bromobenzene (50 mg, 0.31 mmol) in 2 mL of THF was first cooled in the coldwell filled with liquid nitrogen. A hexane solution of *n*-BuLi (0.12 mL, 2.5 M) was added, and the reaction was stirred in the coldwell for 30 min. The reaction mixture was then added dropwise to *N,N′*-diisopropylcarbodiimide (DIC) (39 mg, 0.31 mmol). The colorless solution was stirred inside the coldwell for another 30 min and then added dropwise to $[Ir(btiq)_2(\mu\text{-Cl})]_2$ (53 mg, 0.031 mmol) in 2 mL of THF. After stirring at room temperature for 2 h, the volatiles were removed. The crude product was redissolved in a minimum amount of THF and slowly added to pentane to precipitate out the dark green solid. The product was triturated with diethyl ether and pentane. Yield: 12 mg (19%). ^{1}H NMR (500 MHz, C_6D_6) δ: 9.54 (d, J = 8.5 Hz, 2H, ArH), 9.21 (d, J = 9.0 Hz, 2H, ArH), 8.28 (d, J = 8.0 Hz, 2H, ArH), 8.17 (d, J = 8.0 Hz, 2H, ArH), 7.41 (t, J = 7.0 Hz, 4H, ArH), 7.35 (t, J = 7.8 Hz, 2H, ArH), 7.25 (t, J = 7.5 Hz, 2H, ArH), 7.06 (t, J = 7.8 Hz, 2H, ArH), 7.01 (d, J = 8.5 Hz, 2H, ArH), 6.64−6.69 (m, 3H, ArH), 6.56 (t, J = 7.5 Hz, 2H, ArH), 6.50−6.53 (m, 2H, ArH), 6.22 (t, J = 7.5 Hz, 2H, ArH), 3.37 (quint, J = 6.3 Hz, 2H, $(CH_3)_2CHN$), 0.67 (d, J = 6.5 Hz, 6H, CH_3), 0.059 (d, J = 6.0 Hz, 6H, CH_3). HRMS-ESI (m/z): [M + Na]+ calcd for $C_{55}H_{43}IrN_4S_2$, 1039.2452; found, 1039.2469.

Synthesis of btph-hpp

In the glovebox, $[Ir(btph)_2(\mu\text{-Cl})]_2$ (50 mg, 0.030 mmol) and hppK (13 mg, 0.074 mmol) in 3.0 mL of THF were placed inside a microwave tube. The flask was set up in the microwave reactor. After 10 min of microwave irradiation at 150 °C (5−7 bar), the resulting dark red solution was cooled to room temperature. The solvent was evaporated, and the resulting residue was extracted with 5.0 mL of toluene and filtered through Celite. The toluene was removed in vacuo. The residue was dissolved in minimum amount of THF, and pentane was slowly added to precipitate out the dark red solids. The solids were filtered and dried under vacuum. Yield: 23 mg (41%). ^{1}H NMR (600 MHz, C_6D_6) δ: 9.57 (d, J = 7.2 Hz, 2H, ArH), 8.24 (dd, J = 8.4, 14 Hz, 4H, ArH), 8.04 (d, J = 8.4 Hz, 2H, ArH), 7.51 (d, J = 7.2 Hz, 2H, ArH), 7.40 (dt, J = 7.2, 41 Hz, 4H, ArH), 7.03 (t, J = 7.2 Hz, 4H, ArH), 6.78 (t, J = 8.1 Hz, 2H, ArH), 6.67 (t, J = 7.2 Hz, 2H, ArH), 6.26 (t, J = 7.8 Hz, 2H, ArH), 2.87−2.95 (m, 2H, CH_2), 2.47−2.56 (m, 2H, CH_2), 1.88 (s, 2H, CH_2), 1.69 (s, 2H, CH_2), 1.16 (s, 2H, CH_2), 0.84 (s, 2H, CH_2). This compound was unstable under ambient conditions and thus decomposed while preparing the sample for HRMS. The molecular ion peak was not observed in the mass spectrometry experiment, and only the peak for $[Ir(btph)_2]^+$ ($[M-hpp]^+$; m/z 813.1) was clearly observed.

■ ASSOCIATED CONTENT

Supporting Information

The Supporting Information is available free of charge at https://pubs.acs.org/doi/10.1021/acsorginorgau.1c00044.

https://doi.org/10.1021/acsorginorgau.1c00044
ACS Org. Inorg. Au 2022, 2, 236−244

X-ray crystallography details, cyclic voltammograms, UV−vis absorption and excitation spectra, and NMR spectra (PDF)

Accession Codes

CCDC 2117450−2117452 contain the supplementary crystallographic data for this paper. These data can be obtained free of charge via www.ccdc.cam.ac.uk/data_request/cif, or by emailing data_request@ccdc.cam.ac.uk, or by contacting The Cambridge Crystallographic Data Centre, 12 Union Road, Cambridge CB2 1EZ, UK; fax: +44 1223 336033.

AUTHOR INFORMATION

Corresponding Author

Thomas S. Teets − *Department of Chemistry, University of Houston, Houston, Texas 77204-5003, United States;* orcid.org/0000-0002-7471-8467; Email: tteets@uh.edu

Authors

Po−Ni Lai − *Department of Chemistry, University of Houston, Houston, Texas 77204-5003, United States*

Sungwon Yoon − *Department of Chemistry, University of Houston, Houston, Texas 77204-5003, United States*

Yumeng Wu − *Department of Chemistry, University of Houston, Houston, Texas 77204-5003, United States;* orcid.org/0000-0002-0205-0728

Complete contact information is available at: https://pubs.acs.org/10.1021/acsorginorgau.1c00044

Author Contributions

The manuscript was written through contributions of all authors. All authors have given approval to the final version of the manuscript.

Notes

The authors declare no competing financial interest.

ACKNOWLEDGMENTS

The authors thank the National Science Foundation (Grant CHE-1846831) and the Welch Foundation (Grant E-1887) for funding this research. Y.W. acknowledges the Welch Summer Scholar Program for a research fellowship. We thank Prof. Randy Thummel for access to the microwave reactor.

REFERENCES

(1) Prier, C. K.; Rankic, D. A.; MacMillan, D. W. C. Visible Light Photoredox Catalysis with Transition Metal Complexes: Applications in Organic Synthesis. *Chem. Rev.* **2013**, *113* (7), 5322−5363.

(2) Shon, J.-H.; Kim, D.; Rathnayake, M. D.; Sittel, S.; Weaver, J.; Teets, T. S. Photoredox Catalysis on Unactivated Substrates with Strongly Reducing Iridium Photosensitizers. *Chem. Sci.* **2021**, *12*, 4069−4078.

(3) Bozic-Weber, B.; Constable, E. C.; Housecroft, C. E. Light Harvesting with Earth Abundant D-Block Metals: Development of Sensitizers in Dye-Sensitized Solar Cells (DSCs). *Coord. Chem. Rev.* **2013**, *257* (21−22), 3089−3106.

(4) Polo, A. S.; Itokazu, M. K.; Murakami Iha, N. Y. Metal Complex Sensitizers in Dye-Sensitized Solar Cells. *Coord. Chem. Rev.* **2004**, *248*, 1343−1361.

(5) Teets, T. S.; Nocera, D. G. Photocatalytic Hydrogen Production. *Chem. Commun.* **2011**, *47* (33), 9268−9274.

(6) Mills, I. N.; Porras, J. A.; Bernhard, S. Judicious Design of Cationic, Cyclometalated Ir(III) Complexes for Photochemical Energy Conversion and Optoelectronics. *Acc. Chem. Res.* **2018**, *51* (2), 352−364.

(7) Ma, D.-L.; Ma, V. P.-Y.; Chan, D. S.-H.; Leung, K.-H.; He, H.-Z.; Leung, C.-H. Recent Advances in Luminescent Heavy Metal Complexes for Sensing. *Coord. Chem. Rev.* **2012**, *256* (23−24), 3087−3113.

(8) Liu, Z.; He, W.; Guo, Z. Metal Coordination in Photoluminescent Sensing. *Chem. Soc. Rev.* **2013**, *42* (4), 1568.

(9) *Iridium(III) in Optoelectronic and Photonics Applications*; Zysman-Colman, E., Ed.; John Wiley & Sons, Inc: Chichester, England, 2017.

(10) *Highly Efficient OLEDs with Phosphorescent Materials*; Yersin, H., Ed.; Wiley-VCH: Weinheim, Germany, 2008.

(11) Baldo, M. A.; O'Brien, D. F.; You, Y.; Shoustikov, A.; Sibley, S.; Thompson, M. E.; Forrest, S. R. Highly Efficient Phosphorescent Emission from Organic Electroluminescent Devices. *Nature* **1998**, *395*, 151−154.

(12) Sajoto, T.; Djurovich, P. I.; Tamayo, A. B.; Oxgaard, J.; Goddard, W. A.; Thompson, M. E. Temperature Dependence of Blue Phosphorescent Cyclometalated Ir(III) Complexes. *J. Am. Chem. Soc.* **2009**, *131* (28), 9813−9822.

(13) Lamansky, S.; Djurovich, P.; Murphy, D.; Abdel-Razzaq, F.; Kwong, R.; Tsyba, I.; Bortz, M.; Mui, B.; Bau, R.; Thompson, M. E. Synthesis and Characterization of Phosphorescent Cyclometalated Iridium Complexes. *Inorg. Chem.* **2001**, *40* (7), 1704−1711.

(14) Sasabe, H.; Takamatsu, J.; Motoyama, T.; Watanabe, S.; Wagenblast, G.; Langer, N.; Molt, O.; Fuchs, E.; Lennartz, C.; Kido, J. High-Efficiency Blue and White Organic Light-Emitting Devices Incorporating a Blue Iridium Carbene Complex. *Adv. Mater.* **2010**, *22* (44), 5003−5007.

(15) Kim, D. H.; Cho, N. S.; Oh, H.-Y.; Yang, J. H.; Jeon, W. S.; Park, J. S.; Suh, M. C.; Kwon, J. H. Highly Efficient Red Phosphorescent Dopants in Organic Light-Emitting Devices. *Adv. Mater.* **2011**, *23* (24), 2721−2726.

(16) Lee, J.; Chen, H.-F.; Batagoda, T.; Coburn, C.; Djurovich, P. I.; Thompson, M. E.; Forrest, S. R. Deep Blue Phosphorescent Organic Light-Emitting Diodes with Very High Brightness and Efficiency. *Nat. Mater.* **2016**, *15* (1), 92−98.

(17) Pal, A. K.; Krotkus, S.; Fontani, M.; Mackenzie, C. F. R.; Cordes, D. B.; Slawin, A. M. Z.; Samuel, I. D. W.; Zysman-Colman, E. High-Efficiency Deep-Blue-Emitting Organic Light-Emitting Diodes Based on Iridium(III) Carbene Complexes. *Adv. Mater.* **2018**, *30* (50), 1804231.

(18) Na, H.; Cañada, L. M.; Wen, Z.; Wu, J. I.-C.; Teets, T. S. Mixed-Carbene Cyclometalated Iridium Complexes with Saturated Blue Luminescence. *Chem. Sci.* **2019**, *10* (25), 6254−6260.

(19) Tsuboyama, A.; Iwawaki, H.; Furugori, M.; Mukaide, T.; Kamatani, J.; Igawa, S.; Moriyama, T.; Miura, S.; Takiguchi, T.; Okada, S.; Hoshino, M.; Ueno, K. Homoleptic Cyclometalated Iridium Complexes with Highly Efficient Red Phosphorescence and Application to Organic Light-Emitting Diode. *J. Am. Chem. Soc.* **2003**, *125* (42), 12971−12979.

(20) Fan, C.-H.; Sun, P.; Su, T.-H.; Cheng, C.-H. Host and Dopant Materials for Idealized Deep-Red Organic Electrophosphorescence Devices. *Adv. Mater.* **2011**, *23* (26), 2981−2985.

(21) Lamansky, S.; Djurovich, P.; Murphy, D.; Abdel-Razzaq, F.; Lee, H.-E.; Adachi, C.; Burrows, P. E.; Forrest, S. R.; Thompson, M. E. Highly Phosphorescent Bis-Cyclometalated Iridium Complexes: Synthesis, Photophysical Characterization, and Use in Organic Light Emitting Diodes. *J. Am. Chem. Soc.* **2001**, *123* (18), 4304−4312.

(22) Ho, C.-L.; Li, H.; Wong, W.-Y. Red to Near-Infrared Organometallic Phosphorescent Dyes for OLED Applications. *J. Organomet. Chem.* **2014**, *751*, 261−285.

(23) Yoshihara, T.; Murayama, S.; Masuda, T.; Kikuchi, T.; Yoshida, K.; Hosaka, M.; Tobita, S. Mitochondria-Targeted Oxygen Probes Based on Cationic Iridium Complexes with a 5-Amino-1, 10-Phenanthroline Ligand. *J. Photochem. Photobiol. Chem.* **2015**, *299*, 172−182.

(24) Yoon, S.; Teets, T. S. Red to Near-Infrared Phosphorescent Ir(III) Complexes with Electron-Rich Chelating Ligands. *Chem. Commun.* **2021**, *57* (16), 1975−1988.
(25) Lai, P.-N.; Brysacz, C. H.; Alam, M. K.; Ayoub, N. A.; Gray, T. G.; Bao, J.; Teets, T. S. Highly Efficient Red-Emitting Bis-Cyclometalated Iridium Complexes. *J. Am. Chem. Soc.* **2018**, *140* (32), 10198−10207.
(26) Lai, P.; Teets, T. S. Ancillary Ligand Effects on Red□Emitting Cyclometalated Iridium Complexes. *Chem. Eur. J.* **2019**, *25* (23), 6026−6037.
(27) Kabir, E.; Wu, Y.; Sittel, S.; Nguyen, B.-L.; Teets, T. S. Improved Deep-Red Phosphorescence in Cyclometalated Iridium Complexes *via* Ancillary Ligand Modification. *Inorg. Chem. Front.* **2020**, *7* (6), 1362−1373.
(28) Ikawa, S.; Yagi, S.; Maeda, T.; Nakazumi, H.; Fujiwara, H.; Koseki, S.; Sakurai, Y. Photo- and Electroluminescence from Deep-Red- and near-Infrared-Phosphorescent Tris-Cyclometalated Iridium-(III) Complexes Bearing Largely π-Extended Ligands. *Inorg. Chem. Commun.* **2013**, *38*, 14−19.
(29) Kesarkar, S.; Mróz, W.; Penconi, M.; Pasini, M.; Destri, S.; Cazzaniga, M.; Ceresoli, D.; Mussini, P. R.; Baldoli, C.; Giovanella, U.; Bossi, A. Near-IR Emitting Iridium(III) Complexes with Heteroaromatic β-Diketonate Ancillary Ligands for Efficient Solution-Processed OLEDs: Structure-Property Correlations. *Angew. Chem., Int. Ed.* **2016**, *55* (8), 2714−2718.
(30) Lai, P.-N.; Yoon, S.; Teets, T. S. Efficient Near-Infrared Luminescence from Bis-Cyclometalated Iridium(III) Complexes with Rigid Quinoline-Derived Ancillary Ligands. *Chem. Commun.* **2020**, *56* (62), 8754−8757.
(31) Lu, G.-Z.; Wu, R.; Liu, L.; Zhou, L.; Zheng, Y.-X.; Zhang, W.-W.; Zuo, J.-L.; Zhang, H. A Series of Red Iridium(III) Complexes Using Flexible Dithiocarbamate Derivatives as Ancillary Ligands for Highly Efficient Phosphorescent OLEDs. *Mater. Chem. Front.* **2019**, *3* (5), 860−866.
(32) Radwan, Y. K.; Maity, A.; Teets, T. S. Manipulating the Excited States of Cyclometalated Iridium Complexes with β-Ketoiminate and β-Diketiminate Ligands. *Inorg. Chem.* **2015**, *54* (14), 7122−7131.
(33) Shon, J.-H.; Sittel, S.; Teets, T. S. Synthesis and Characterization of Strong Cyclometalated Iridium Photoreductants for Application in Photocatalytic Aryl Bromide Hydrodebromination. *ACS Catal.* **2019**, *9* (9), 8646−8658.
(34) Lu, G.-Z.; Su, N.; Yang, H.-Q.; Zhu, Q.; Zhang, W.-W.; Zheng, Y.-X.; Zhou, L.; Zuo, J.-L.; Chen, Z.-X.; Zhang, H.-J. Rapid Room Temperature Synthesis of Red Iridium(III) Complexes Containing a Four-Membered Ir−S−C−S Chelating Ring for Highly Efficient OLEDs with EQE over 30%. *Chem. Sci.* **2019**, *10* (12), 3535−3542.
(35) Cotton, F. A.; Donahue, J. P.; Lichtenberger, D. L.; Murillo, C. A.; Villagrán, D. Expeditious Access to the Most Easily Ionized Closed-Shell Molecule, $W_2(Hpp)_4$. *J. Am. Chem. Soc.* **2005**, *127* (31), 10808−10809.
(36) Shon, J.-H.; Kim, D.; Gray, T. G.; Teets, T. S. β-Diketiminate-Supported Iridium Photosensitizers with Increased Excited-State Reducing Power. *Inorg. Chem. Front.* **2021**, *8* (13), 3253−3265.
(37) Carlson, G. A.; Djurovich, P. I.; Watts, R. J. Widely Varying Photophysical Properties of Ligand-Nitrated Bis(μ-Chloro)Tetrakis-(2-Phenylpyridinato)Diiridium(III). *Inorg. Chem.* **1993**, *32* (21), 4483−4484.
(38) Colombo, M. G.; Brunold, T. C.; Riedener, T.; Guedel, H. U.; Fortsch, M.; Buergi, H.-B. Facial Tris Cyclometalated Rhodium(3+) and Iridium(3+) Complexes: Their Synthesis, Structure, and Optical Spectroscopic Properties. *Inorg. Chem.* **1994**, *33* (3), 545−550.
(39) Yersin, H.; Rausch, A. F.; Czerwieniec, R.; Hofbeck, T.; Fischer, T. The Triplet State of Organo-Transition Metal Compounds. Triplet Harvesting and Singlet Harvesting for Efficient OLEDs. *Coord. Chem. Rev.* **2011**, *255* (21−22), 2622−2652.
(40) Yoshihara, T.; Kobayashi, A.; Oda, S.; Hosaka, M.; Takeuchi, T.; Tobita, S. Iridium Complex Probes for Monitoring of Cellular Oxygen Levels and Imaging of Hypoxic Tissues. *SPIE BiOS* **2012**, 82330A.
(41) Nonoyama, M. Benzo[h]Quinolin-10-Yl-N Iridium(III) Complexes. *Bull. Chem. Soc. Jpn.* **1974**, *47* (3), 767−768.
(42) Baus, J. A.; Tacke, R. Neutral Six-Coordinate Bis-(Dithiocarbamato)Silicon(IV) Complexes with an $SiCl_2S_4$ Skeleton. *Dalton Trans.* **2017**, *46* (27), 8751−8755.
(43) Seybold, P. G.; Gouterman, M. Porphyrins. *J. Mol. Spectrosc.* **1969**, *31*, 1−13.
(44) Sheldrick, G. M. Crystal Structure Refinement with *SHELXL*. *Acta Crystallogr. Sect. C Struct. Chem.* **2015**, *71* (1), 3−8.
(45) Spek, A. L. Structure Validation in Chemical Crystallography. *Acta Crystallogr. D Biol. Crystallogr.* **2009**, *65* (2), 148−155.

https://doi.org/10.1021/acsorginorgau.1c00044
ACS Org. Inorg. Au 2022, 2, 236−244